Talanta 119 (2014) 306–311

Contents lists available at ScienceDirect

Talanta

journal homepage: www.elsevier.com/locate/talanta

Specific and sensitive colorimetric detection of Al^{3+} using 5-mercaptomethyltetrazole capped gold nanoparticles in aqueous solution

Dingshuai Xue*, Hongyue Wang, Yanbin Zhang

Institute of Geology and Geophysics, Chinese Academy of Sciences, Beijing 100029, China

ARTICLE INFO

Article history:
Received 11 August 2013
Received in revised form
27 October 2013
Accepted 1 November 2013
Available online 13 November 2013

Keywords:
Al^{3+}
Colorimetric detection
Gold nanoparticles
5-mercaptomethyltetrazole

ABSTRACT

Contamination of food and drinking water by health-risk levels of Al^{3+} calls for convenient assays. Here, we report a method to visibly detect Al^{3+} at room temperature. Firstly, the chelating ligand of 5-mercaptomethyltetrazole (MMT) was synthesized and modified on the surface of AuNPs through the strong Au–S interaction to form a MMT–AuNP probe, which can remain well-dispersed and stable in an aqueous solution for a long time. Upon the addition of Al^{3+}, the interparticle crosslinking induced aggregation (color change from red to blue) of MMT–AuNPs was triggered through the Al^{3+}–MMT interaction. Under optimal conditions, the absorbance ratio (A_{620}/A_{520}) of MMT–AuNPs is linear within the Al^{3+} concentration range from 1.0 to 10.0 μM, and the detection limit (3σ) was as low as 0.53 μM. Moreover, an interference study showed that this MMT–AuNP probe discriminated Al^{3+} from a wide range of environmentally dominant metal ions and anions. The practical utility of the new method was demonstrated by determining Al^{3+} in several environmental water and human urine specimens, obtaining satisfactory results. Being a rapid, convenient and cost-effective method, it should become a powerful alternative to conventional methods for selective quantification of Al^{3+} in routine laboratory practice or rapid on-site assay.

1. Introduction

The widespread use of aluminum in food additives, pharmaceuticals, aluminum foil, vessels, and trays results in contamination of food and drinking water by hazardous levels of Al^{3+} inevitably. A number of epidemiologic studies speculated the unintentionally chronic low-dose exposure to Al^{3+} to account for many health issues. For example, Al^{3+} can accumulate in the bone causing bone softening and atrophy as well as other abnormalities. It affects iron absorption in the blood by competitively binding with iron binding proteins and further causing anemia [1]. In addition, Al^{3+} has been implicated as a causative factor in Alzheimer's disease and is associated with damage to the central nervous system in humans [2,3]. To avoid the adverse health problems caused by the uptake of Al^{3+}, an estimated tolerable dietary intake in the human body is 7 mg kg^{-1} body weight per week [4]. Therefore, developing convenient and economic assay for Al^{3+} is highly desirable especially for rural and remote areas.

Al^{3+} is detected using multiple laboratory analysis platforms, including HPLC–MS, inductively coupled plasma (ICP)-MS and atomic fluorescence spectroscopy (AFS) [5,6]. Although these methods can enable a high level of qualitative and quantitative analyses, operative inability by a non-specialist and requirement of sophisticated instrumentation severely limit applications which are suitable for point-of-care, field deployment, or other low-resource settings.

To date, optical sensors, especially the colorimetric ones, have always been the most convenient analytical tool and gained a lot of interest because they provide a simple and economical assay without the aid of instruments. In recent years, colorimetric chemosensors have been widely exploited for Al^{3+} detection [7–9], which depends on the rational design of Al^{3+}-responsive receptors with sufficient or even remarkable sensitivity and selectivity. Although they provide a straightforward and acceptable assay, they always suffer from complicated probe design, multistep synthesis strategy and large reagent consumption. Besides, concerning their practical applications, aqueous media may be the best choice for Al^{3+} detection, but majority of these sensors are unstable or dysfunctional in aqueous solution.

Compared with the well-developed chromophoric chemosensors, gold nanoparticles (AuNPs) based colorimetric assays have recently emerged as a fascinating research field [10–13]. AuNPs

* Corresponding author. Tel.: +86 10 82998487; fax: +86 10 62010846.
E-mail address: xuedingshuai@mail.iggcas.ac.cn (D. Xue).

0039-9140/$ - see front matter © 2013 Elsevier B.V. All rights reserved.
http://dx.doi.org/10.1016/j.talanta.2013.11.012

can be synthesized in a straightforward manner and remain highly stable after proper surface modification. They possess unique optical properties which depend on interparticle distance, *i.e.* aggregation/redispersion is directly observed as a solution color switch due to surface plasmon coupling. This spectral shift property coupled with the high extinction coefficient of AuNPs (from 1×10^{8} to $1\times10^{10}\,M^{-1}\,cm^{-1}$), which is often several orders of magnitude higher than those of organic dyes, allows for an easy colorimetric assay of a wide range of targets, including metal ions, small molecules, proteins, nucleic acids, malignant cells, *etc.*, at fairly low concentrations. Prior to their use as sensing tools, AuNPs must usually be chemically tailored and their structures or surface functional properties need to be modified for specific molecular interaction. Although a large number of sensitive and reliable AuNPs based colorimetric detections of transition metal ions (Cd^{2+}, Pb^{2+}, Hg^{2+}, Cu^{2+}, *etc.*) have been introduced [14–20], the colorimetric Al^{3+} sensing using AuNP probe is not well studied. Li et al. reported the first colorimetric assay based on pentapeptide functionalized AuNPs for detecting Al^{3+}, which achieved great success at monitoring contaminated levels of Al^{3+} on living cellular surfaces [21]. Moreover, mononucleotide-modified metal nanoparticles were also reported as a colorimetric probe for selective and sensitive detection of Al^{3+} and used to monitor Al^{3+} on living cellular surfaces under physiological conditions [22].

To develop a convenient alternative for on-site Al^{3+} assay that meets the requirements of low cost, high sensitivity and selectivity, water compatibility and environment friendliness, we demonstrated a colorimetric assay for the detection of Al^{3+} at room temperature with remarkably high sensitivity and selectivity. 5-mercaptomethyltetrazole (MMT) was synthesized and introduced as the chelating ligand on the surface of AuNPs (Scheme 1). We found that MMT–AuNPs could selectively bind to Al^{3+} rather than other metal cations. In aqueous media, the affinity of Al^{3+} toward the functional tetrazole group led to an interparticle crosslinking induced aggregation of MMT–AuNPs and a clear color change from red to blue. Therefore, a sensitive and selective colorimetric assay for visually detecting Al^{3+} is developed, which could aid in evaluating dangerous levels of Al^{3+} in water sources. Compared with the use of pentapeptide or mononucleotide modified AuNPs as the Al^{3+} probe [21,22], this small molecular ligand-modified AuNP probe is cheaper and readily achievable. More importantly, the MMT–AuNP probe could well match the proposed probes in terms of its sensing capacity.

2. Material and method

2.1. Instruments

Transmission electron microscope (TEM) measurements were performed on a H-7500 instrument (Hitachi). Absorption spectra were recorded on a double-beam Du-800 UV–vis spectrophotometer (Beckman). The zeta potential was measured by a Zeta sizer Nano ZS90 apparatus (Malvern, UK). Raman measurements were conducted in a Renishaw InVia Raman spectrometer at an excitation laser of 785 nm. Thermo Scientific ELEMENT 2 ICP-MS was used to detect Al^{3+} in real samples. Nuclear magnetic resonance (NMR) data of the synthesized ligand were collected using a Bruker Avance-600 MHz NMR spectrometer.

2.2. Chemicals

Chloroauric acid ($HAuCl_4$) was obtained from Aldrich Chemicals and used as received. Other chemicals used were of analytical grade or of the highest purity available. All the solutions were prepared using Milli-Q water (Millipore) as the solvent. The certified reference materials, including ground water (BCR-609) and river water (LGC6019), were bought from the LGC Standards.

2.3. Synthesis of 5-mercaptomethyltetrazole

According to previous reported literature [23,24], MMT was synthesized by the cycloaddition of sodium azide to chloroacetonitrile

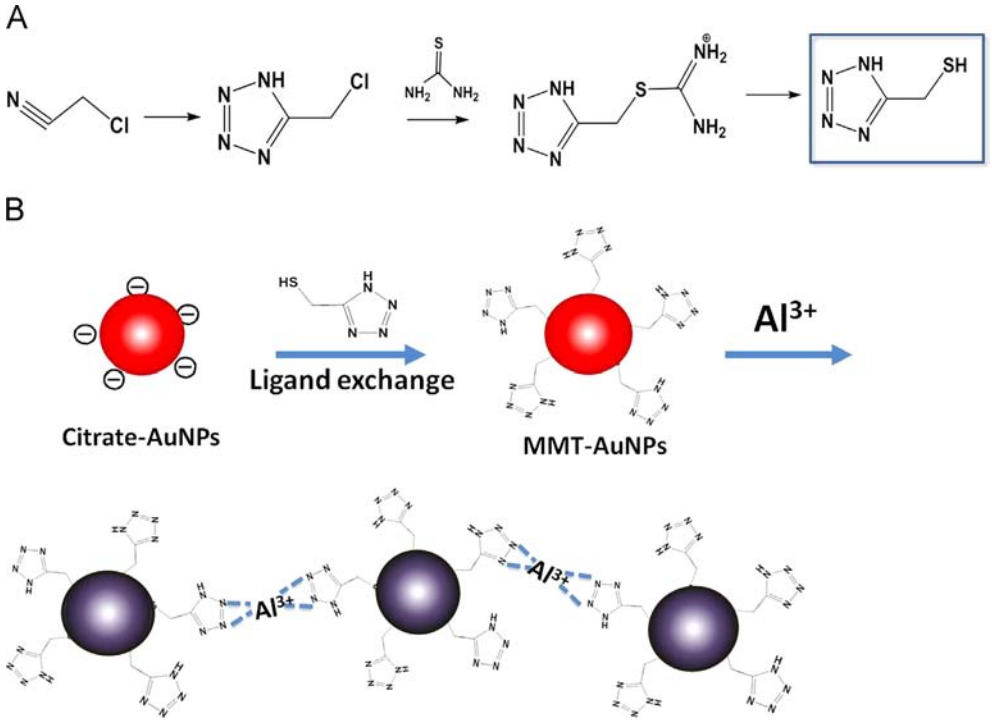

Scheme 1. (A) Synthesis of 5-mercaptomethyltetrazole (MMT). (B) Illustration of ligand exchange of MMT on the surface of AuNPs and signaling strategy for Al^{3+} based on the MMT–AuNP probe.

followed by the replacement of chlorine atom by the hydrosulfide group under the treatment of 5-chloromethyltetrazole with thiourea as shown in Scheme 1(A). The resulting ligand was characterized by ^{1}H and ^{13}C NMR spectroscopy.

2.4. Synthesis of 5-mercaptomethyltetrazole capped AuNPs

Uniform 12 nm AuNPs were prepared through a facile one-step approach by citrate mediated reduction of $HAuCl_4$ in aqueous solutions [25]. The synthesized AuNPs are capped with MMT directly through S–Au binding. In detail, the AuNPs solution (10.0 mL, 10 nM) was mixed with different amounts of MMT (50 mM) under pH 10.5 with continued stirring for 48 h. To remove unbound MMT, the solution was centrifuged for 20 min at 12,000 rpm and washed with supernatants. After two wash/centrifuge cycles, the MMT–AuNPs were recovered separately in ultrapure water and kept at 4 °C. The concentration of the AuNPs can be calculated according to Beer's law using an extinction coefficient of $2.4\times10^{8}\ M^{-1}\ cm^{-1}$ at 520 nm for the 12 nm AuNPs [26]. The resulting MMT–AuNPs were characterized using TEM, UV–vis, and Raman spectroscopy.

2.5. Surface ligand characterization using Raman spectroscopy

Silicon wafers (5 mm × 5 mm) were washed twice in water, sonicated in ethanol/water (1:1) for 5 min, and finally immerged in piranha solution (30% H_2O_2 and concentrated H_2SO_4, 1:3 volume; caution: strong oxidizing agent) for 30 min. The wafers were then washed with water and ethanol, blown dry with N_2 and heated at 120 °C for 2 h in an oven. Different AuNPs were purified by centrifugation twice, dropped on silica wafer slide, and allowed to air-dry at room temperature. Then, spectra were collected. The system was automatically calibrated against a silicon wafer peak at 520 cm^{-1}. During the measurements, a 50× objective was used, and the laser spot diameter was 30 μm. All samples were measured with 140 mW laser power and 10 s acquisition time, and a baseline correction was performed for all measurements.

2.6. Signal response of MMT–AuNP probe to Al^{3+}

A 2.5 mL MMT–AuNPs aqueous solution buffered with 10 mM Tris–HCl, pH 8.0 was spiked with 0.5 mL Al^{3+} solutions to produce final concentrations in the range of 1.0–10.0 μM. The mixtures were then reacted at room temperature for 15 min and transferred for absorbance and photograph collection. The absorption ratios of A_{620}/A_{520} *versus* Al^{3+} concentrations were used for calibration.

2.7. Detection of Al^{3+} in real samples

Tap and well water samples were collected from Beijing and Zhangbei county of Hebei province, respectively. Human urine samples were collected randomly from five healthy people and filtered through a 0.22 μm microporous membrane. A five-fold diluted solution of filtrate urine was then used for the detection of Al^{3+} according to the general procedure without additional special treatment. In a typical process, 1.0 mL of the sample spiked with Al^{3+} standard solutions was added to 2.0 mL of MMT–AuNPs solution (10 mM Tris–HCl, pH 8.0). After 15 min, the colorimetric measurement was performed.

3. Results and discussion

3.1. Characterization of 5-mercaptomethyltetrazole

MMT was characterized by ^{1}H and ^{13}C NMR spectroscopy (Figs. S1 and S2 in supporting information). It presents a white solid melting at 69–70 °C. ^{1}H NMR (400 MHz, DMSO-D_6): δ 3.38 (^{1}H, t, J=8.2 MHz, HS), 4.03 (^{2}H, d, J=8.2 MHz, CH_2); ^{13}C NMR (125 MHz, DMSO-D_6): δ 29.18 (CH_2), 154.0 ($C_{tetrazole}$). Anal. calcd. $C_2H_4N_4S$: C 20.68, H 3.47, N 48.24, and S 27.61. Found: C 20.33, H 3.26, N 48.68, and S 27.57.

3.2. Characterization of the MMT–AuNP probe

To demonstrate the utility of this approach, 12 nm-diameter AuNPs were employed to fabricate the probe, and then the MMT ligand was linked to them through ligand exchange. In this process, initially weakly adsorbed citrate on the AuNPs was replaced by the stronger binding MMT ligand. The characteristics of citrate and MMT capped AuNPs have been compared based on their shapes, surface plasma peaks and Raman spectra fingerprints. Both citrate and MMT capped AuNPs are well dispersed and have the same average diameter of 12 nm (Fig. 1A and B), but the surface plasma peak of the latter shows a slight red-shift from 519 nm to 520 nm upon modification of MMT (Fig. 1C) because of the increase of the surrounding refractive index.

Surface enhanced Raman scattering (SERS) emerges as a useful technique for characterizing adsorption of many organic molecules on some metal colloids, mainly Au and Ag. In this experiment, the

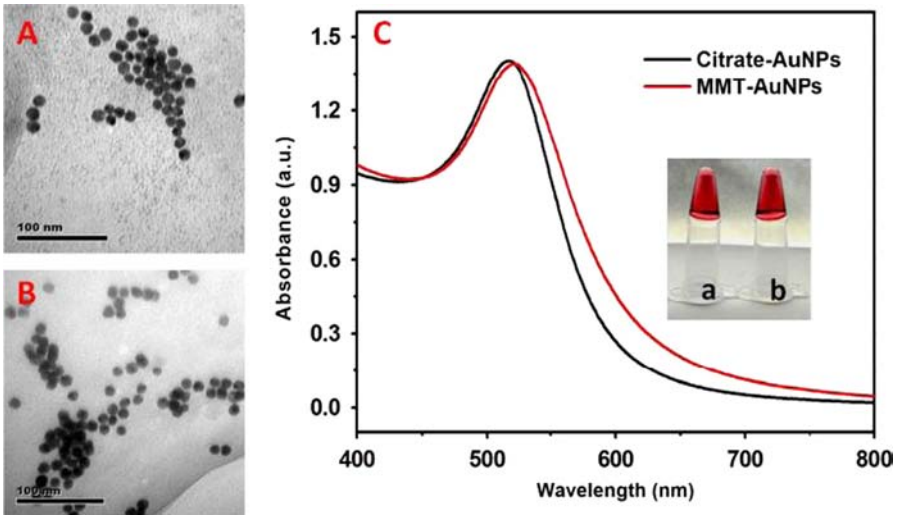

Fig. 1. (A) TEM images of citrate and (B) MMT capped AuNPs. (C) Absorbance spectra of citrate and MMT capped AuNPs. Both are dispersed in aqueous solution at 3.5 nM.

strong, characteristic MMT vibrational SERS signals have been obtained for the MMT–AuNPs (Fig. 2). In detail, the enhanced peaks can be associated with the vibrational modes from the C–S groups, for example, at 1226 and 889 cm^{-1}, and the peak at 1017 cm^{-1} is associated with the N–N vibrational modes. Moreover, the vibration signatures centered at approximately 1414 and 1475 cm^{-1} have major contributions from the C–C (bridge-head carbon atoms) and C–N stretching. The characteristic signature of the Au–S stretching mode is clearly visible in the SERS spectra at 240 cm^{-1}, which clearly indicates the exclusive coordinative interaction of the MMT molecule with the AuNPs through its thiol group. In contrast, the citrate ligand shows weak SERS spectra, which is blamed for its small Raman cross section.

3.3. Stability of the MMT–AuNPs in salt solution

Applications of sensors are usually performed in complex environments with high concentration of salts, which would result in irreversible aggregation of AuNPs. It is found that the strong interaction of MMT ligand could provide sufficient stability for AuNPs rather than citrate in salt solution. As shown in Fig. S3, the absorbance spectra of the MMT–AuNPs solution (3.5 nM) remained almost unaltered in the presence of NaCl as high as 30 mM. However, obvious color change occurred immediately in the case of citrate–AuNPs upon exposure to the same amount of salt concomitant with reduced absorbance and significant red-shift of the LSPR band due to aggregation. The well-dispersed feature of the MMT–AuNPs may be attributed to the electrostatic and steric stability provided by the anionic charges on MMT and the organosulfur monolayer.

Furthermore, long-term stability is also an important property for the AuNP probe. After 6 months storage at 4 °C, the MMT–AuNPs solution did not show a significant spectral change in comparison with the freshly-prepared one (data not shown). These results demonstrate that the MMT–AuNPs exhibit better stability against environmental changes, making them more suitable in practical application.

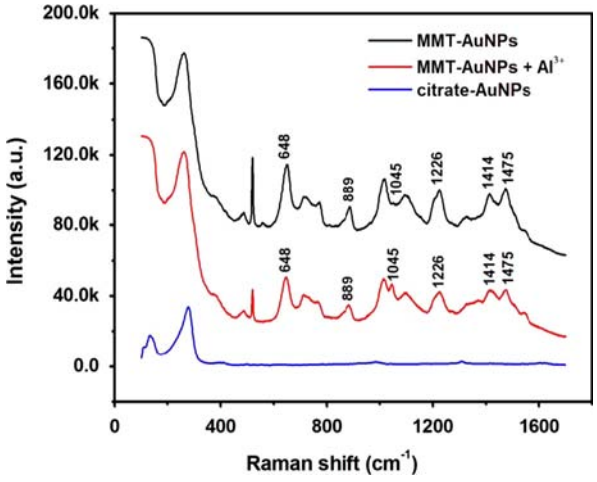

Fig. 2. SERS spectra of citrate, MMT ligand on AuNPs, and MMT–AuNPs obtained by adding Al^{3+}. The experiment conditions have been described in the Material and method section.

3.4. Principle for Al^{3+} induced aggregation of MMT–AuNPs

Typically, the MMT–AuNPs exhibit an absorption maximum at 520 nm in aqueous solution. Notably, when titrated with Al^{3+}, this band decreased gradually and was accompanied by the generation of a new absorption peak at 620 nm with the distinct color change from red to steel blue, which mirrored those of the well-dispersed MMT–AuNPs that suffered from aggregation (Fig. 3). This phenomenon indicates that the MMT–AuNPs can be used as a colorimetric indicator for Al^{3+}.

To further confirm the dispersion status of MMT–AuNPs, we compared their TEM images. As expected, the addition of Al^{3+} induced obvious aggregation (Fig. 3). This observation is also supported by the DLS data. The average hydrodynamic diameter of well-dispersed MMT–AuNPs is 28.3 nm, which increases to 302.8 nm in the presence of Al^{3+} (10 μM). This result is consistent with the UV–vis and TEM analyses. Moreover, the zeta potential of the MMT–AuNPs dispersion is −27.1 mV at pH 8.0. With the addition of Al^{3+} (10 μM), the values increase to +2.2 mV, which suggests that the complex of Al^{3+}–MMT is formed on the surface of AuNPs, and Al^{3+} partially shields the surface charge of the AuNPs and increases the van der Waals attractive forces among them.

The change of SERS spectra could provide more evidence to confirm the interaction between Al^{3+} and MMT–AuNPs. Compared with the SERS spectra of MMT–AuNPs (Fig. 2), a new peak at 1045 cm^{-1} appears after adding Al^{3+}, which corresponds to the N–N vibrational mode. This result reflects the interaction of Al^{3+}

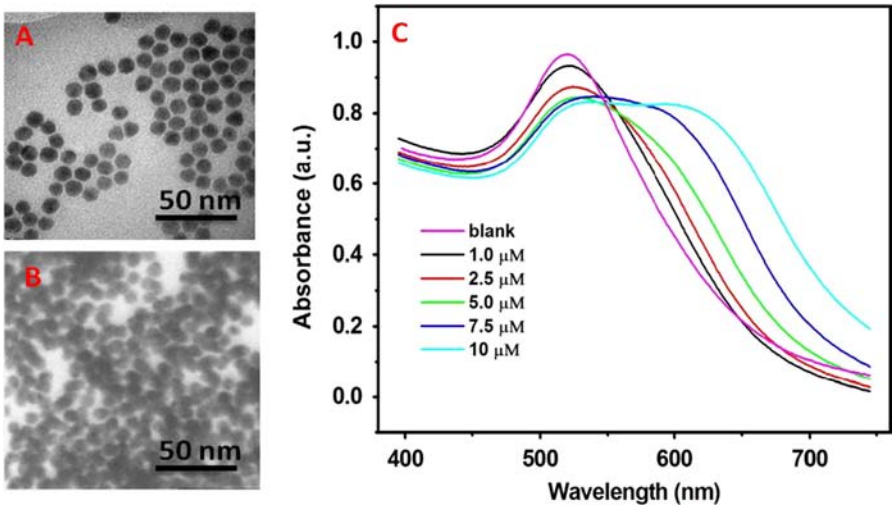

Fig. 3. (A) TEM images of MMT–AuNPs dispersion (3.5 nM) and (B) after its exposure to 10 μM Al^{3+}. (C) Absorbance spectra of MMT–AuNPs (3.5 nM) solutions upon gradual addition of varied concentrations of Al^{3+}. All of them were buffered in 10 mM Tris–HCl at pH 8.0.

with N atoms in a tetrazole ring, in which the N_2 and N_3 atoms prefer to bind Al^{3+} (alkaline earth metal ions) with regard to acid/base hardness.

Based on the above research, we propose a possible mechanism of this phenomenon. Presumably, the tetrazolate anion is generated by deprotonation of the 5-monosubstituted tetrazole (pKa 4.8) under pH 8.0, which is known to be a bridging ligand to coordinate with alkaline earth metal ions by the N_2 and N_3 atoms of the tetrazole ring [27,28]. Therefore, we speculate that the unique complexion ability of the tetrazole enables Al^{3+} to interact with N-donor sites; thus, a fast and efficient interparticle cross-linking of the MMT–AuNPs occurs. Scheme 1(B) summarizes the procedure for the working mechanism of the MMT–AuNPs probe.

3.5. Optimal conditions

Aggregation of the MMT–AuNPs is attributed to the complexion between Al^{3+} and MMT molecules on the surface of AuNPs; therefore, it is reasonable that an appropriate surface density of MMT ligand is significant to this process. As shown in Fig. S4, increasing addition of MMT while keeping the AuNPs at a constant concentration in the ligand exchange process, the sensitivity of the resulting probe increased gradually to the best signal response and then remained constant. This result demonstrated that the high surface density of MMT has a positive effect on sensitivity. Therefore, we choose the MMT concentration at 150 μM, which is nearly 4×10^4 in excess to that of AuNPs, as the optimal ligand concentration.

Impact of pH on the assay was also investigated. When the pH value is less than 5.0, the MMT–AuNPs are unstable and aggregated easily, so the effect of pH ranging from 5.0 to 9.0 was studied here (Fig. S5). The color changes of MMT–AuNPs become more and more obvious from pH 5.0 to 8.0 after adding increased amounts of Al^{3+} and then decrease gradually. This phenomenon may be due to the strong alkaline solution which results in the formation of aluminum hydroxide precipitate. Finally, we chose pH 8.0 as the final condition, considering the preferable sensitivity.

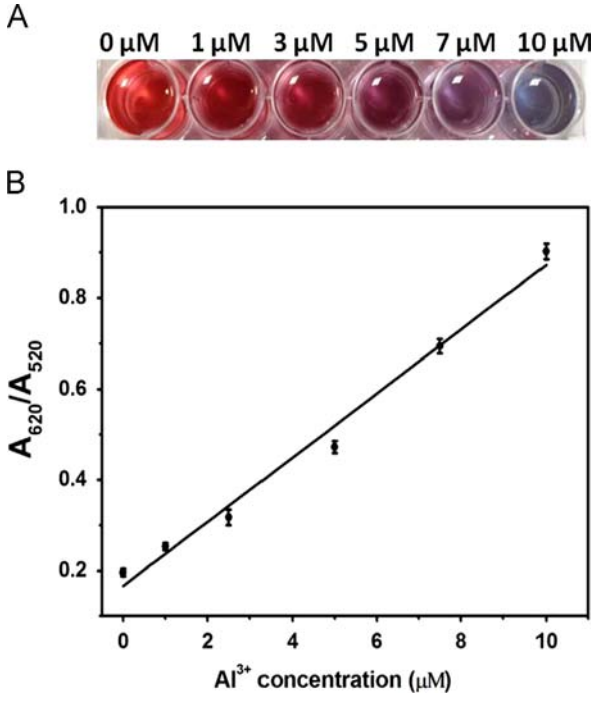

Fig. 4. (A) Photograph of the MMT–AuNP color after adding different amounts of standard Al^{3+} solution. (B) Plot of the absorption ratios A_{620}/A_{520} against Al^{3+} concentration in the range of 1.0–10.0 μM for quantitative detection; each point reflects the average of three independent experiments. Error bars indicate standard deviations. (For interpretation of the references to color in this figure legend,the reader is referred to the web version of this article.)

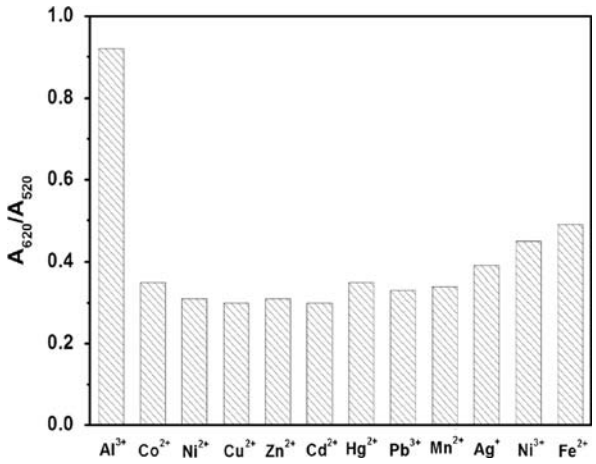

Fig. 5. Signal response of MMT–AuNPs toward various metal ions. Concentrations: Al^{3+} 10 μM; other metal ions, 1.0 mM.

Table 1
Results for the determination of Al^{3+} in water and human urine samples.

Samples	Blank value[a] (μM)	Added (μM)	Detection value[b] (μM)	Recovery (%)	Standard deviation
Tap water	0.12	10.0	10.19	102	± 0.2
Well water	0.66	10.0	10.73	107	± 0.3
Human urine 1	0.032	10.0	10.22	102	± 0.5
Human urine 2	0.047	10.0	10.26	103	± 0.4
Human urine 3	0.021	10.0	10.17	102	± 0.5
Human urine 4	0.025	10.0	10.20	102	± 0.4

[a] Detection using ICP-MS and the value is mean of three determinations.
[b] Mean of three determinations.

Furthermore, a time course study indicates that the complex of Al^{3+} with MMT–AuNPs at room temperature occurs quickly and can reach a plateau within 10 min (Fig. S6). For achieving better reproducibility, the reaction time of 15 min is employed in our experiments.

Under optimal conditions, the sensitivity of the MMT–AuNP probe for Al^{3+} was investigated. It is demonstrated that the values of A_{620}/A_{520} show a linear dependence on Al^{3+} concentration after incubating for 15 min (Fig. 4). As shown in Fig. 5, the absorbance ratios (A_{620}/A_{520}) of MMT–AuNPs can be fitted to the equation $A_{620}/A_{520}=0.166+0.071C$ (Al^{3+}, μM) over the range from 1.0 to 10 μM, $R^2=0.9927$. The limit of detection (3σ) for Al^{3+} is calculated as 0.53 μM, which is much lower than the level (7.4 μM) of drinking water defined by the World Health Organization [29] and comparable to that of the pentapeptide functionalized AuNP probe [21,22].

3.6. Selectivity and analytical application

To evaluate the specificity of the MMT–AuNPs probe, the signal response to various interferences was examined in buffer solution. Color screening against other metal ions (Fig. 5) indicated that the relatively large amounts of other metal ions have a small influence on this assay. Moreover, the presence of Na^+, K^+, F^-, Cl^-, Br^-, I^-, Ac^-, CO_3^{2-}, NO_3^-, PO_4^{3-} and SO_4^{2-}, which are abundant in water, does not result in a distinct color change of MMT–AuNPs, although the concentrations of those ions reached as high as 5.0 mM. Overall, this finding suggests that the normally

encountered anion and environmental substrates do not pose a problem in the quantitative detection of Al^{3+}. The method was further validated by determining Al^{3+} concentration in the certified reference materials. As shown in Table S1, the obtained values are well-matched with the certified ones. These results demonstrated that the MMT–AuNP probe could enable a simple and accurate assay for Al^{3+}.

All the linearity and selectivity studies show that the MMT–AuNP probe could be used for the detection of Al^{3+} in complex matrix. Here, both environmental water and urine were chosen to evaluate the application of the probe for the detection of Al^{3+}. Thereafter, the real samples spiked with certain amounts of Al^{3+} were determined according to the standard curve, and the results are listed in Table 1. It is suggested that the present method may be used in the detection of Al^{3+} in water quality monitoring and in urine sample testing.

4. Conclusions

In summary, a simple, cost-effective colorimetric assay for Al^{3+} based on the MMT modified AuNPs is developed in this paper. The MMT–AuNP probe was achieved by the ligand exchange process, and it shows improved stability over that of the primary citrate–AuNPs. It is demonstrated that the affinity of Al^{3+} toward the N atom of the tetrazole group induces the aggregation of MMT–AuNPs following by distinct solution color change. The MMT–AuNPs probe possesses better anti-interference ability with the detection limit (3σ) as low as 0.53 μM. The probe is successfully applied for sensing residual Al^{3+} in water and human urine samples. Because this method can address intrinsic limitations of small molecular-based optical sensors, such as complex synthesized procedures, low-sensitivity and poor water compatibility, it can find great application in selective quantification of Al^{3+} in routine laboratory practice or rapid on-site assay.

Appendix A. Supplementary material

Supplementary data associated with this article can be found in the online version at http://dx.doi.org/10.1016/j.talanta.2013.11.012.

References

[1] B. Valeur, I. Leray, Coord. Chem. Rev. 205 (2000) 3–40.
[2] Z. Krejpcio, R.W. Wojciak, Pol. J. Environ. Stud. 11 (2002) 251–254.
[3] G.D. Fasman, Coord. Chem. Rev. 149 (1996) 125–165.
[4] P. Nayak, Environ. Res. 89 (2002) 111–115.
[5] P.M. Bertsch, M.A. Anderson, Anal. Chem. 61 (1989) 35–36.
[6] B. Fairman, A. Sanz-Medel, P. Jones, E.H. Evans, Analyst 123 (1998) 699–703.
[7] M. Arduini, F. Felluga, F. Mancin, P. Rossi, P. Tecilla, U. Tonellato, N. Valentinuzzi, Chem. Commun. 13 (2003) 1606–1607.
[8] D. Maity, T. Govindaraju, Chem. Commun. 46 (2010) 4499–4501.
[9] S. Kim, J.Y. Noh, K.Y. Kim, J.H. Kim, H.K. Kang, S.W. Nam, S.H. Kim, S. Park, C. Kim, J. Kim, Inorg. Chem. 51 (2012) 3597–3602.
[10] R. Elghanian, J.J. Storhoff, R.C. Mucic, R.L. Letsinger, C.A. Mirkin, Science 277 (1997) 1078–1081.
[11] J. Liu, Y. Lu, Nat. Protoc. 1 (2006) 246–252.
[12] J.S. Lee, P.A. Ulmann, M.S. Han, C.A. Mirkin, Nano Lett. 8 (2008) 529–533.
[13] K. Saha, S.S. Agasti, C. Kim, X. Li, V.M. Rotello, Chem. Rev. 112 (2012) 2739–2779.
[14] J. Liu, Y. Lu, J. Am. Chem. Soc. 125 (2003) 6642–6643.
[15] J.S. Lee, M.S. Han, C.A. Mirkin, Angew. Chem. Int. Ed. 46 (2007) 4093–4096.
[16] D. Li, A. Wieckowska, I. Willner, Angew. Chem. Int. Ed. 47 (2008) 3927–3931.
[17] Y. Zhou, S. Wang, K. Zhang, X. Jiang, Angew. Chem. Int. Ed. 47 (2008) 7454–7456.
[18] D. Liu, W. Qu, W. Chen, W. Zhang, Z. Wang, X. Jiang, Anal. Chem. 82 (2010) 9606–9610.
[19] Y. Xue, H. Zhao, Z. Wu, X. Li, Y. He, Z. Yuan, Analyst 136 (2011) 3725–3730.
[20] Y. Guo, Z. Wang, W. Qu, H. Shao, X. Jiang, Biosens. Bioelectron. 26 (2011) 4064–4069.
[21] X. Li, J. Wang, L. Sun, Z. Wang, Chem. Commun. 46 (2010) 988–990.
[22] M. Zhang, Y.Q. Liu, B.C. Ye, Chem. Eur. J. 18 (2012) 2507–2513.
[23] V. Lesnyak, S.V. Voitekhovich, P.N. Gaponik, N. Gaponik, A. Eychmüller, ACS Nano 4 (2010) 4090–4096.
[24] L.I. Vereshchagin, A.V. Petrov, V.N. Kizhnyaev, F.A. Pokatilov, A.I. Smirnov, Russ. J. Org. Chem. 42 (2006) 1049–1055.
[25] K.C. Grabar, R.G. Freeman, M.B. Hommer, M.J. Natan, Anal. Chem. 67 (1995) 735–743.
[26] J.J. Storhoff, R. Elghanian, R.C. Mucic, C.A. Mirkin, R.L. Letsinger, J. Am. Chem. Soc. 120 (1998) 1959–1964.
[27] H. Zhao, Z.R. Qu, H.Y. Ye, R.G. Xiong, Chem. Soc. Rev. 37 (2008) 84–100.
[28] V. Lesnyak, A. Wolf, A. Dubavik, L. Borchardt, S.V. Voitekhovich, N. Gaponik, S. Kaskel, A. Eychmüller, J. Am. Chem. Soc. 133 (2011) 13413–13420.
[29] Guidelines for Drinking Water Quality, World Health Organization, three ed., 397 Geneva, 2004, pp. 301-311.